Journal of Materials Chemistry C

PAPER

View Article Online
View Journal | View Issue

Cite this: J. Mater. Chem. C, 2018, 6, 10751

Nonstoichiometry, structure, and properties of $Ba_{1-x}TiO_y$ thin films†

Arvind Dasgupta,[ab] Sahar Saremi,[a] Xu Ruijuan,[a] Liv R. Dedon,[ab] Shishir Pandya,[a] Anoop R. Damodaran[a] and Lane W. Martin*[a]

Received 4th June 2018,
Accepted 7th September 2018

DOI: 10.1039/c8tc02725k

rsc.li/materials-c

The effects of growth conditions on the chemistry, structure, electrical leakage, dielectric response, and ferroelectric behavior of $Ba_{1-x}TiO_y$ thin films are explored. Although single-phase, coherently-strained films are produced in all cases, small variations in the laser fluence during pulsed-laser deposition growth result in films with chemistries ranging from $BaTiO_3$ to $Ba_{0.93}TiO_{2.87}$. As the laser fluence increases, the films become more barium deficient and the out-of-plane lattice parameter expands (as much as 5.4% beyond the expected value for $Ba_{0.93}TiO_{2.87}$ films). Stoichiometric $BaTiO_3$ films are found to be three orders of magnitude more conducting than $Ba_{0.93}TiO_{2.87}$ films and the barium-deficient films exhibit smaller low-field permittivity, lower loss tangents, and higher dielectric maximum temperatures. Although large polarization is observed in all cases, large built-in potentials (shifted loops) and hysteresis-loop pinching are present in barium-deficient films – suggesting the presence of defect dipoles. The effects of these defect dipoles on ferroelectric hysteresis are studied using first-order reversal curves. Temperature-dependent current–voltage and deep-level transient spectroscopy studies reveal at least two defect states, which grow in concentration with increasing deficiency of both barium and oxygen, at ~0.4 eV and ~1.2 eV above the valence band edge, which are attributed to $V''_{Ba} - V^{\bullet\bullet}_{O}$ defect–dipole complexes and V''_{Ba} defect states, respectively. The defect states can also be removed *via ex post facto* processing. Such work to understand and control defects in this important material could provide a pathway to enable better control over its properties and highlight new avenues to manipulate functions in these complex materials.

Introduction

For a material to be technologically relevant, it is imperative that one can repeatedly produce and control that material to exhibit the desired properties and functions. In this regard, defects, which are fundamentally inherent to materials, are often seen as detrimental to the both material properties and reliability and, thus, much effort has focused on reducing the concentration or deterministically controlling the nature of defects. But, when controlled thoughtfully, defects can provide improved performance.[1] The classic example is semiconductors such as silicon which are of limited utility in their intrinsic state, but when purposefully doped, provide the foundation for modern electronics. In electroceramics, neither the exacting control of materials chemistry (which can readily approach ppb levels in silicon) nor exacting doping methodologies are widespread. Instead, the approach has been to alloy materials with rather large concentrations of species to counteract any deleterious properties that would be present from intrinsic defects. This brute force approach exposes a general deficiency in the understanding of and ability to probe defects in complex ceramic systems and precludes a more nuanced defect-engineering approach for shaping material properties.

In, for example, ferroelectric ceramics, defects have been extensively studied and are known to strongly affect a number of critical parameters including leakage,[2] fatigue,[3] and dielectric properties.[4] This is especially true in the case of the prototypical oxide ferroelectric $BaTiO_3$, which is widely used as a dielectric material for multilayer ceramic capacitors[5] and piezoelectric actuators and transducers.[6,7] As such, it is almost never used in its pure form, and is often alloyed with a wide variety of species in order to tune and elicit useful and stable responses.[8,9] Thus, efforts have centered on the introduction of extrinsic defects to counterbalance the defects present in the "pristine" material. Considerably less work, however, has been focused on the thoughtful use of intrinsic defects to solve material challenges. Advances in material synthesis – including thin-film deposition approaches – now provide for more exacting control over materials which enables the deterministic creation of intrinsic-defect

[a] Department of Materials Science and Engineering, University of California, Berkeley, Berkeley, CA 94720, USA. E-mail: lwmartin@berkeley.edu
[b] Materials Sciences Division, Lawrence Berkeley National Laboratory, Berkeley, CA 94720, USA

† Electronic supplementary information (ESI) available. See DOI: 10.1039/c8tc02725k

structures in complex materials like the perovskite oxides[10,11] and, in turn, allows for the study of defect–property coupling. In particular, in the case of pulsed-laser deposition, intrinsic-defect control *via* knock-on damage[12,13] and stoichiometry[14–16] have been used to dramatically affect material properties. At the same time, innovative materials processing steps are now being envisioned for *ex post facto* control of defect structures including defect introduction[13,17] and healing.[18] In the case of $BaTiO_3$, intrinsic defects created by the synthesis process have been used to develop colossal permittivity in ceramics produced by spark-plasma[19] and microwave-assisted sintering.[20] Though the exact mechanism for this colossal permittivity is unclear, it has been attributed to the presence of barium and oxygen vacancies.[21] Ultimately, exerting control over the stoichiometry and defects and, more importantly, knowing how chemistry and defects can be effectively utilized to control materials, can open up a new horizon of materials control in complex materials.

Here, the effects of growth conditions on the film chemistry, structure, electrical leakage, dielectric response, and ferroelectric behavior of $Ba_{1-x}TiO_y$ thin films are explored. Although single-phase, coherently-strained films are produced in all cases, small variations in the laser fluence during pulsed-laser deposition result in films with chemistries ranging from $BaTiO_3$ to $Ba_{0.93}TiO_{2.87}$. In turn, as the laser fluence increases and the films become more barium deficient, the out-of-plane lattice parameter expands (as much as 5.4% beyond a stoichiometric value of 4.069 Å[22] for $Ba_{0.93}TiO_{2.87}$ films). Stoichiometric $BaTiO_3$ films are found to be three orders of magnitude more conducting than $Ba_{0.93}TiO_{2.87}$ films and the barium-deficient films exhibit smaller low-field permittivity, lower loss tangents, and higher dielectric maximum temperatures. Although large polarization is observed in all cases, large built-in potentials (shifted loops) and hysteresis-loop pinching are present in barium-deficient films – suggesting the presence of defect dipoles. The effect of these defect dipoles on ferroelectric hysteresis was also studied using first-order reversal curves. Temperature-dependent current–voltage and deep-level transient spectroscopy studies reveal at least two defect states at $\sim$0.4 eV and $\sim$1.2 eV above the valence band that grow in concentration with increasing deficiency of both barium and oxygen. *Ex situ* introduction of additional oxygen vacancies and barium allows for further understanding of the nature of the defects and their role in driving structural and property evolution. The defect states are attributed to shallow $V''_{Ba} - V^{\bullet\bullet}_{O}$ defect–dipole complexes and deep V''_{Ba} defect states, which can be removed *via ex post facto* processing. Ultimately, such work to understand and control defects in this important material could provide a pathway to enable better control over its properties and highlight new avenues to manipulate functions in these complex materials.

Experimental section

100 nm-thick $Ba_{1-x}TiO_y$ thin films were grown *via* pulsed-laser deposition (KrF excimer laser, 248 nm; LPX 305, Coherent) in an on-axis geometry (5.5 cm target-to-substrate spacing) on 30 nm-thick $SrRuO_3$-buffered $GdScO_3(110)$ single-crystal substrates (CrysTec GmBH). The $SrRuO_3$ films, used as a bottom electrode for electrical characterization, were grown from a $SrRuO_3$ ceramic target at a heater temperature of 700 °C in a dynamic-oxygen pressure of 100 mTorr, with a laser fluence of 1.1 J cm^{-2}, and at a laser repetition rate of 15 Hz. The $Ba_{1-x}TiO_y$ films were grown from a $BaTiO_3$ ceramic target at a heater temperature of 600 °C in a dynamic-oxygen pressure of 40 mTorr, with laser fluences of 1.25, 1.45, and 1.65 J cm^{-2} at a laser repetition rate of 2 Hz. The laser fluence was varied by increasing the energy of the laser pulse while maintaining the spot size. All substrates were attached to the heater with silver paint (Ted Pella, Inc.), and all films were cooled at a rate of 5 °C min^{-1} to ambient temperature in a static-oxygen pressure of 700 Torr.

Following growth, a variety of techniques were used to probe the structural, chemical, and electrical/dielectric/ferroelectric properties. X-ray diffraction (X'Pert^3 MRD, Panalytical) studies including symmetric on-axis line scans and asymmetric off-axis reciprocal space maps were completed. The stoichiometry of the films was measured using Rutherford backscattering spectrometry (RBS) with a He-ion beam with an incident energy of 3.040 MeV, an incident angle of $\alpha = 22.5°$, an exit angle $\beta = 25.35°$, and a scattering angle $\theta = 168°$. The samples used for RBS were grown on MgO substrates (CrysTec GmBH) in order the prevent overlap of the film peaks with the rare-earth peaks from the scandate substrates. Fits to the experimental RBS data were completed using the analysis software SIMNRA, and the quality of the fit was evaluated using an R^2 method. In order to prevent overfitting and artificially large R^2 values, the R^2 values were evaluated only in the regions near the peaks and were calculated individually for each of the different peaks. Following a methodology reported previously,[15] operation at an incident ion-beam energy of 3.040 MeV, which corresponds to the oxygen resonance energy wherein oxygen has an increased scattering cross-section and thus high-scattering intensities, allows for the simultaneous extraction of anion stoichiometry. We note, however, that to limit the influence of nonresonance scattering from oxygen in the substrate, reliable information on the film can only be extracted from the top $\sim$45 nm, and hence reported values of oxygen stoichiometry herein should be noted in this regard (additional details in the ESI†). Finally, although we are confident with cation chemistries to 1–2% accuracy (that is a change in $A_1B_1O_3$ cation chemistry by 0.01 out of 1), difficulty in fitting the low-energy tail of the resonant peaks renders accurate reporting to better than $\sim$3% (that is a change in $A_1B_1O_3$ anion chemistry of 0.1 out of 3) difficult.

Top $SrRuO_3$ electrodes (50 nm thickness and 25 μm diameter circular capacitors) were grown *ex situ* using an established MgO hard-mask process.[23] Current–voltage (leakage) studies were measured using an unswitched triangular-voltage profile (which uses a prepoling pulse to remove contributions from switching currents; Precision Multiferroic Tester, Radiant Technologies, Inc.). Dielectric properties were measured using an impedance analyzer (E4990A, Keysight Technologies) as a function of frequency and temperature. Rayleigh measurements of dielectric constant *versus* excitation voltage were also used to determine the reversible regime and an excitation field of 1 kV cm^{-1}

(identified to be safely inside the reversible regime) was used for all measurements. Ferroelectric switching measurements (Precision Multiferroic Tester, Radiant Technologies, Inc.) were performed using a bipolar triangular voltage profile at various frequencies (0.1–10 kHz). First-order reversal curve (FORC) measurements were carried out by measuring multiple minor loops starting from a fixed negative voltage with a saturated polarization and increasing maximum fields (E_r). They were performed at 10 kHz using a monopolar triangular voltage profile. Deep-level transient spectroscopy measurements (Precision Multiferroic Tester, Radiant Technologies, Inc.) were carried out in a temperature-dependent, vacuum-probe station (Lake Shore Cryotronics) from 100 to 400 K. A 5 V pulse was applied for 10 ms as the trap-filling pulse and the subsequent capacitance decay transient was measured. The boxcar method with multiple time windows[24] was used to extract the trap energies.

Some of the $Ba_{1-x}TiO_y$ films grown at a laser fluence of 1.65 J cm^{-2} were also subjected to additional annealing experiments to further elucidate the defect structures and types. One film was annealed at 500 °C at a dynamic oxygen pressure of 1 mTorr for 60 min and then subsequently cooled to ambient temperature in the same pressure. Another sample was subjected to barium reintroduction using a chemical-vapor deposition (CVD)-style setup in a tube furnace in which the film was placed at the end of the hot zone while an alumina boat filled with BaO powder was placed at the beginning of the hot zone. Oxygen was flowed into the furnace first over the BaO powder and towards the film, while the temperature was ramped at a rate of 25 °C min^{-1} to 700 °C, maintained for 60 min at that temperature, and then cooled to ambient temperature at a rate of 5 °C min^{-1}. The sample was then cleaned by sonicating in dilute 0.5 M HCl solution for 5 min to remove excess BaO from the surface before additional X-ray diffraction, RBS, and electrical measurements were completed.

Results and discussion

We begin by discussing the X-ray diffraction results. Wide-angle symmetric θ–2θ line scans reveal single-phase, 00l-oriented, epitaxial films of $Ba_{1-x}TiO_y$ (Fig. 1a). The quality of the thin films is evidenced by the existence of Laue fringes (ESI,† Fig. S1a–c). It is noted that even as the laser fluence is increased, the diffraction peaks arising from the $Ba_{1-x}TiO_y$ films remain sharp and the full-width-at-half-maximum (FWHM) of the rocking curves about the 002-diffraction condition for the films remain essentially the same (0.0254°–0.0291°; ESI,† Fig. S1d–f). The position of the 00l-diffraction conditions for the various $Ba_{1-x}TiO_y$ films is found to be shifted to lower angles (corresponding to an increase in the out-of-plane lattice parameter) as the laser fluence is increased. Further information on this structural change is obtained from reciprocal space mapping

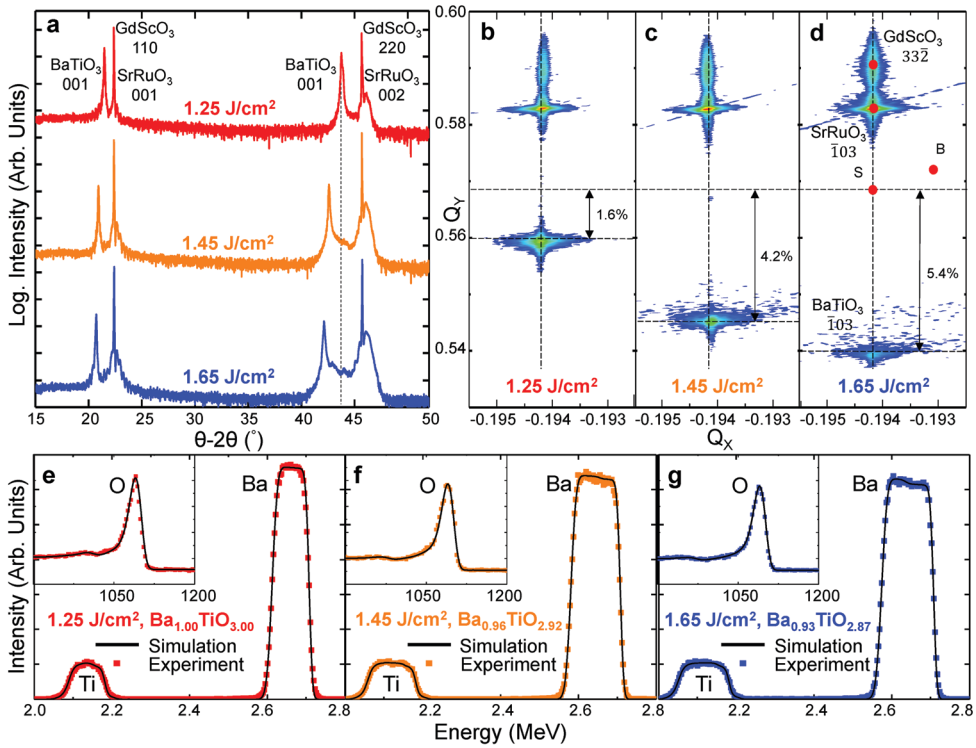

Fig. 1 (a) θ–2θ X-ray diffraction scans of the $Ba_{1-x}TiO_y/SrRuO_3/GdScO_3$(110) heterostructures grown at laser fluences of 1.25 J cm^{-2} (top, red), 1.45 J cm^{-2} (middle, orange), and 1.65 J cm^{-2} (bottom, blue). Off-axis reciprocal space mapping studies about the $\bar{1}03$- and $33\bar{2}$-diffraction conditions of the film and the substrate, respectively, with the heterostructures grown at laser fluences of (b) 1.25 J cm^{-2}, (c) 1.45 J cm^{-2}, and (d) 1.65 J cm^{-2}. Rutherford backscattering spectra with a zoom-in image of the oxygen resonance peak (inset) for heterostructures grown at laser fluences of (e) 1.25 J cm^{-2}, (f) 1.45 J cm^{-2}, and (g) 1.65 J cm^{-2}.

studies about the $\bar{1}03$- and $33\bar{2}$-diffraction conditions of the film and the substrate, respectively (Fig. 1b–d). In all cases, regardless of the laser fluence during growth, the films are found to be coherently strained to the substrate as they have the same values of in-plane lattice parameters. At the same time, a systematic increase in the out-of-plane lattice parameter is seen to extend from 1.6% to 4.2% to 5.4% beyond the theoretically expected strained peak position for $BaTiO_3$ grown on $GdScO_3$ substrates for the films grown at laser fluences of 1.25, 1.45, and 1.65 J cm^{-2}, respectively. This indicates that strain alone cannot account for this significant increase in the out-of-plane lattice parameter. Similar lattice expansion with varying laser fluence during pulsed-laser deposition growth of $BaTiO_3$ thin films has been reported before[12,25] with the cause suggested to be related to defects and non-stoichiometry.

In order to better understand the cause of this lattice expansion, RBS measurements were completed (Fig. 1e–g). The results suggest a systematic decrease in the barium and oxygen contents with increasing laser fluence. The stoichiometry of the films is found to vary from $Ba_{1.00}TiO_{3.00}$ to $Ba_{0.96}TiO_{2.92}$ to $Ba_{0.93}TiO_{2.87}$ for growth at 1.25, 1.45, and 1.65 J cm^{-2}, respectively. This large difference in the chemistry of the films is somewhat surprising, as the crystalline quality of these films is maintained even in the face of ~7% cation nonstoichiometry: a testament to the tolerance of these perovskite materials to defects. In turn, the large expansion in the out-of-plane lattice parameter can likely be ascribed to the lattice distortion created by these defects since cation/anion vacancies are known to typically drive lattice expansion.[10] In this case, since the in-plane lattice parameters are clamped and fixed to the lattice parameters of the substrate, this manifests itself as an accelerated change in the out-of-plane lattice parameter.

Having established that the growth process can be used to vary the cation and anion stoichiometry, while maintaining the production of single-phase, coherently-strained, high-quality films, we proceed to explore the influence of such defects on the leakage, dielectric, and ferroelectric properties. We first investigate the leakage properties of these films (Fig. 2a). Upon increasing the deficiency of both barium and oxygen, there is a reduction of the leakage (~10^3-times smaller in $Ba_{0.93}TiO_{2.87}$). Next, the dielectric permittivity of these films was measured as a function of frequency at ambient temperature from 1 to 100 kHz (Fig. 2b). It is noted that all films exhibit low dielectric loss in this frequency range and little frequency dispersion. The dielectric permittivity is also found to reduce with increasing deficiency of both barium and oxygen, ranging from a value of ~250 for the $Ba_{1.00}TiO_{3.00}$ films to ~175 for the $Ba_{0.93}TiO_{2.87}$ films (at 1 kHz). The dielectric permittivity was also measured as a function of temperature from 25 to 500 °C (Fig. 2c). The maximum in dielectric permittivity (and therefore the Curie temperature T_C) occurs at drastically different temperatures – ranging from ~425 °C for the $Ba_{1.00}TiO_3$ films to values higher in temperature than our measurement system can probe. This variation is likely related to the differences in structure between these films since T_C is directly related to the robustness and stability of the polar order that arises from the tetragonal

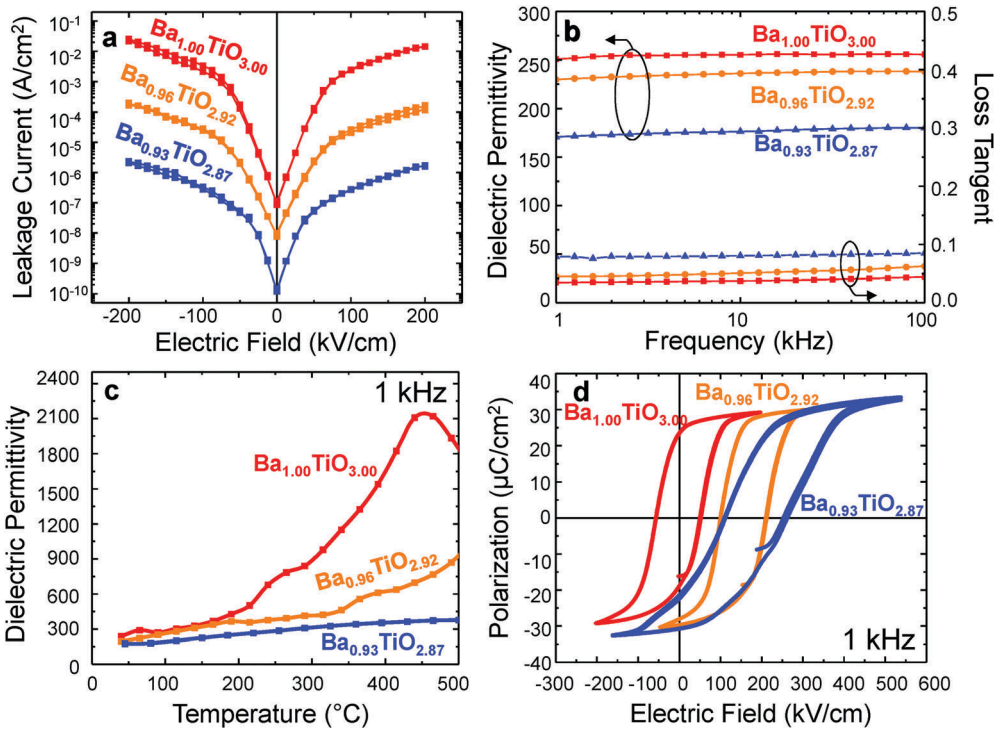

Fig. 2 (a) Room temperature current–voltage (electric field) or leakage measurements, (b) room-temperature, low-field dielectric permittivity (left axis) and loss tangent (right axis), (c) temperature dependence of dielectric permittivity, and (d) polarization-electric field hysteresis loops measured at 1 kHz for $Ba_{1.00}TiO_{3.00}$, $Ba_{0.96}TiO_{2.92}$, and $Ba_{0.93}TiO_{2.87}$ heterostructures.

distortion of the lattice.[22,26] The defects in the nonstoichiometric films give rise to a further enhancement of the out-of-plane lattice parameter, above and beyond the strain introduced by the lattice mismatch with the substrate. This in turn could help explain the variations in the magnitude of the low-field, room-temperature dielectric permittivity; the farther away the material is from T_C, the lower the room-temperature dielectric permittivity one expects.

Finally, polarization-electric field hysteresis loops were measured for the various films at a range of frequencies (for brevity, we show data here at 1 kHz; Fig. 2d). All the films have similar values of saturation polarization ($\sim$30 μC cm^{-2}), but depending on the stoichiometry the films exhibit different built-in potentials (as manifested as a horizontal shift of the hysteresis loop along the voltage axis), which increases with increasing barium and oxygen deficiency. Since all the films are measured with essentially symmetric electrode structures, the cause of this shift is expected to be intrinsic to the ferroelectric itself. This built-in potential could also help explain the variations in the magnitude of the low-field, room-temperature dielectric permittivity; the larger the built-in potential, the less small-scale excitations can do to drive susceptibility and the lower the effective low-field response. It should also be noted that there is an emergence of a slight pinching of the hysteresis loops near the coercive fields in the most barium- and oxygen-deficient films. This is an indicator of the likely presence of defect dipoles (charged point-defect complexes) which can give rise to internal bias fields and loop pinching.[27,28] Defect dipoles in perovskite ferroelectrics are often due to complexes between oxygen vacancies and either *B*-site acceptor dopants[29,30] or *A*-site vacancies.[31]

To further study the impact of these defects on the switching process, FORC measurements[32,33] were carried out to study the internal bias and the coercive-field distribution. One of the most well-accepted methods to mathematically model hysteresis response is the Preisach model.[34,35] This approach relies on defining a basic unit of hysteresis called a hysteron, which is a bi-stable unit with a certain coercive field and internal bias. A statistical distribution of these hysterons within the material can be used to fully describe the hysteresis. The FORC measurements (ESI,† Fig. S2) were completed and contour plots of the internal bias *versus* the coercive field are provided (Fig. 3a–c). Consistent with ferroelectric hysteresis loops, we see that there is an increase in the internal bias of the films as the non-stoichiometry increases. In the most barium- and oxygen-deficient films (Fig. 3c), the peak further splits into two which is characteristic of the pinching present in the hysteresis loop.[36,37] The two peaks are present at similar internal-bias fields, but one is at a higher value of the coercive field. This can be understood by considering that as the non-stoichiometry increases, more defect dipoles are produced and aligned in a direction parallel to the polarization, thereby providing a strong internal bias that manifests itself as a shift in the peak of the hysteron distribution along the internal-bias field axis.[27] At high defect–dipole concentrations, there is an onset of pinching within the films which is commonly believed to be due to stabilization of a domain configuration by the distribution of defect dipoles.[28,38] The defect dipoles pin the domain-wall motion during switching,[39] thereby driving a certain subset of hysterons to a higher value of the coercive field, even while maintaining a similar value of internal bias to the other regions of the film as evidenced by the bimodal distribution of coercive fields. In conclusion, these well-known "fingerprints" of defect dipoles, namely internal bias and loop pinching, are present in the films and vary systematically with non-stoichiometry.

Having studied the effects of these defects on hysteresis, we turn our attention to the effect that they have on the electrical properties. First, temperature-dependent current–voltage measurements were undertaken to study the leakage mechanisms. The raw data (ESI,† Fig. S3) was ultimately found to be the best fit *via* a modified Poole–Frenkel mechanism (Fig. 4a), which is governed by the trapping and de-trapping of carriers by intra-band-gap trap states. It is seen that in all the films, conduction is governed by a trap present at a similar value of $\sim$0.4 eV. p-type conductivity is commonly reported for $BaTiO_3$ at ambient pressure[40] (and, it should be noted, would be reinforced by the presence of additional barium vacancies[41]). This suggests that there is a trap state of $\sim$0.4 eV above the valence band that acts to trap holes within the material, and is present in all films. To further study the intra-gap states, DLTS was utilized (Fig. 4b–d).[24] For the $Ba_{1.00}TiO_{3.00}$ heterostructure (Fig. 4b), only weak, hard to fit, DLTS peaks are observed. Since the temperature-dependent current–voltage studies reveal at least a trap state at $\sim$0.4 eV, we conclude that

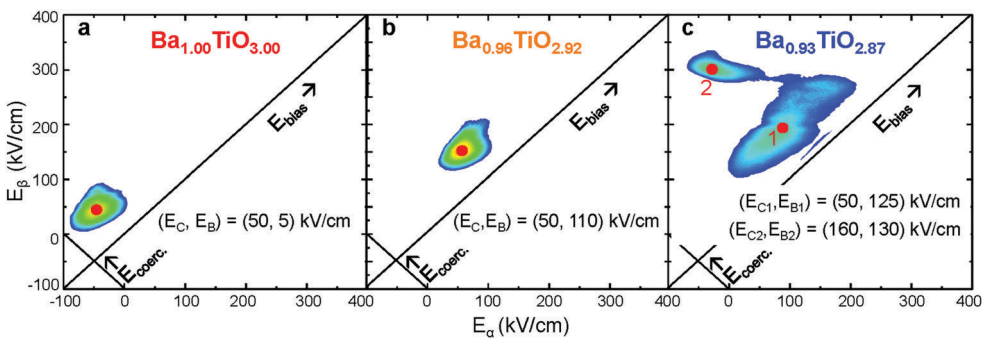

Fig. 3 Distributions of hysterons as extracted from the FORC measurements for (a) $Ba_{1.00}TiO_{3.00}$, (b) $Ba_{0.96}TiO_{2.92}$, and (c) $Ba_{0.93}TiO_{2.87}$ heterostructures.

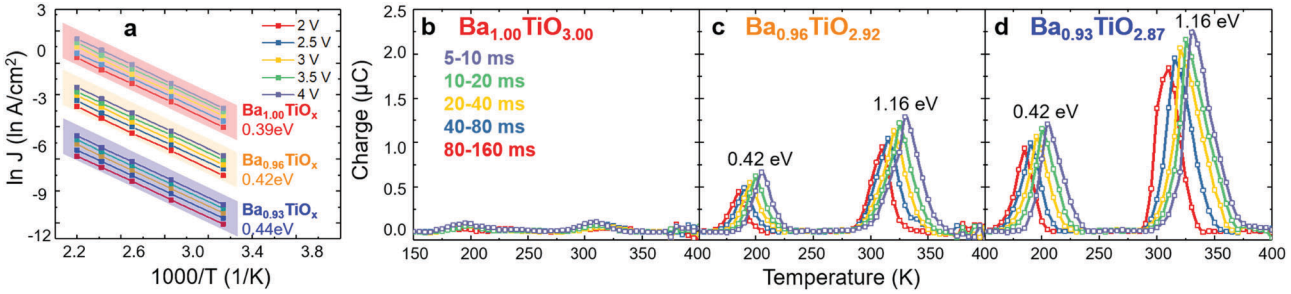

Fig. 4 (a) Poole–Frenkel fits of current–voltage or leakage measurements used to determine the trap energies for the various heterostructures. Dominant trap energies are noted. Deep-level transient spectroscopy data and the extract intragap trap energies for (b) $Ba_{1.00}TiO_{3.00}$, (c) $Ba_{0.96}TiO_{2.92}$, and (d) $Ba_{0.93}TiO_{2.87}$ heterostructures.

since this heterostructure is close to the ideal stoichiometry, that the low defect concentration means that the DLTS signal from these traps is too weak to be readily measured by our setup. We do note that two small peaks are found to extend just above the noise floor that corresponds in location to pronounced peaks discussed later. On the other hand, as the barium and oxygen deficiency is increased in the $Ba_{0.96}TiO_{2.92}$ (Fig. 4c) and $Ba_{0.93}TiO_{2.87}$ (Fig. 4d) heterostructures, two peaks are seen to emerge corresponding to the energies of $\sim$0.4 eV and $\sim$1.2 eV. Furthermore, as the barium and oxygen deficiency increases, so does the concentration of the defect states (as indicated by the increasing peak heights). The shallower defect state (at $\sim$0.4 eV) matches what was extracted as the defect state responsible for the transport behavior from the modified Poole–Frenkel fits (Fig. 4a). Previous theoretical work using ionic potential models[42,43] has shown that V''_{Ba} states can act as a trap for holes and preferentially form complexed with $V^{\bullet\bullet}_{O}$. Experimental work on intra-gap states in $BaTiO_3$ using cathodoluminescence[44] as well as impedance measurements[45] has uncovered a plethora of possible states of which two are relevant to this study, namely, V'_{Ba} and V''_{Ba}, which are thought to occur $\sim$0.6 eV and $\sim$1.2 eV above the conduction band edge. From this, we propose that the defect we observe at $\sim$1.2 eV can be attributed to the existence of V''_{Ba} within our films; however, the defect observed at $\sim$0.4 eV cannot be readily attributed to V'_{Ba}, not only because it does not match the energy but also because previous theoretical[43] and experimental[46,47] studies suggest that this state is likely not favorable and is often unobserved.

For $Ba_{1-x}TiO_y$ films, one might expect the mitigating defect equations to be $\frac{1}{2}O_2 \rightarrow V''_{Ba} + O^{\times}_{O} + 2h^{\bullet}$ or $TiO_2 \rightarrow V''_{Ba} + V^{\bullet\bullet}_{O} + Ti_{Ti} + 2O_O$.[46,48] In the former case, the simple introduction of barium vacancies has the effect of hole doping the lattice (in order to maintain charge neutrality), thereby increasing the carrier concentration. In the latter case, the effects are mitigated by the formation of a Schottky pair,[49,50] where instead of introducing charge carriers, a compensatory defect (an oxygen vacancy) is formed. This is consistent with our observation of increasing oxygen-vacancy concentration as we introduce barium deficiency. Due to electrostatic- and strain-energy considerations, the two charged defects constituting the Schottky pair are complexed with each other to form a more stable ground state,[51,52] likely giving rise to the aforementioned defect dipoles; and the associated internal bias and pinching in the ferroelectric hysteresis loops. Thus, we propose that the trap state observed at $\sim$0.4 eV in the temperature-dependent current–voltage and DLTS studies corresponds to a defect–dipole complex of $V''_{Ba} - V^{\bullet\bullet}_{O}$. This attribution is further supported by theoretical calculations which show that the energy of the $V''_{Ba} - V^{\bullet\bullet}_{O}$ complex should be smaller than that of an isolated V''_{Ba}.[53] This happens since the two defects making the complex are oppositely charged, thus the complex should be less effective at trapping carriers and is closer to the band edge.

Combining these observations, it is possible to posit an explanation as to why the leakage current drops as the barium and oxygen deficiency is increased. In dielectric films, leakage can depend on a variety of factors including carrier concentration, effective mass, mobility, mean free path, and trap concentrations.[54] In our case, due to the compensatory-defect mechanism, the first three factors (concentration, effective mass, and mobility) are expected to remain the same as there is no electron or hole doping which is introduced and the majority carrier type remains the same. Instead, it is the last two, namely, mean free path and trap concentration which are changing within our films. Non-donor traps are known to reduce leakage in dielectric films[54,55] by reducing the mean free path between trapping/detrapping events. So, it is likely through this mechanism that the leakage in our films is decreased and it illustrates the power of introducing intrinsic defects in $BaTiO_3$.

To further confirm our attribution of the defect states, we explored *ex situ* means to control the chemistry and simultaneously monitor trap states *via* DLTS, thereby helping us to conclusively identify them. Details of the DLTS studies and extraction of trap-state energies are provided elsewhere (ESI,† Fig. S4). For this section, we focus on the most defective $Ba_{0.93}TiO_{2.87}$ heterostructures (Fig. 5a). First, the effect of driving down the concentrations of oxygen vacancies was probed by annealing the film at 500 °C for 60 min at an oxygen pressure of 760 Torr. This oxygen annealing, however, had essentially no effect on the film – the structure, chemistry, leakage properties, and DLTS spectra remained effectively unchanged (data not shown here for brevity). This can be rationalized by considering the fact that the oxygen vacancies are stable because they are

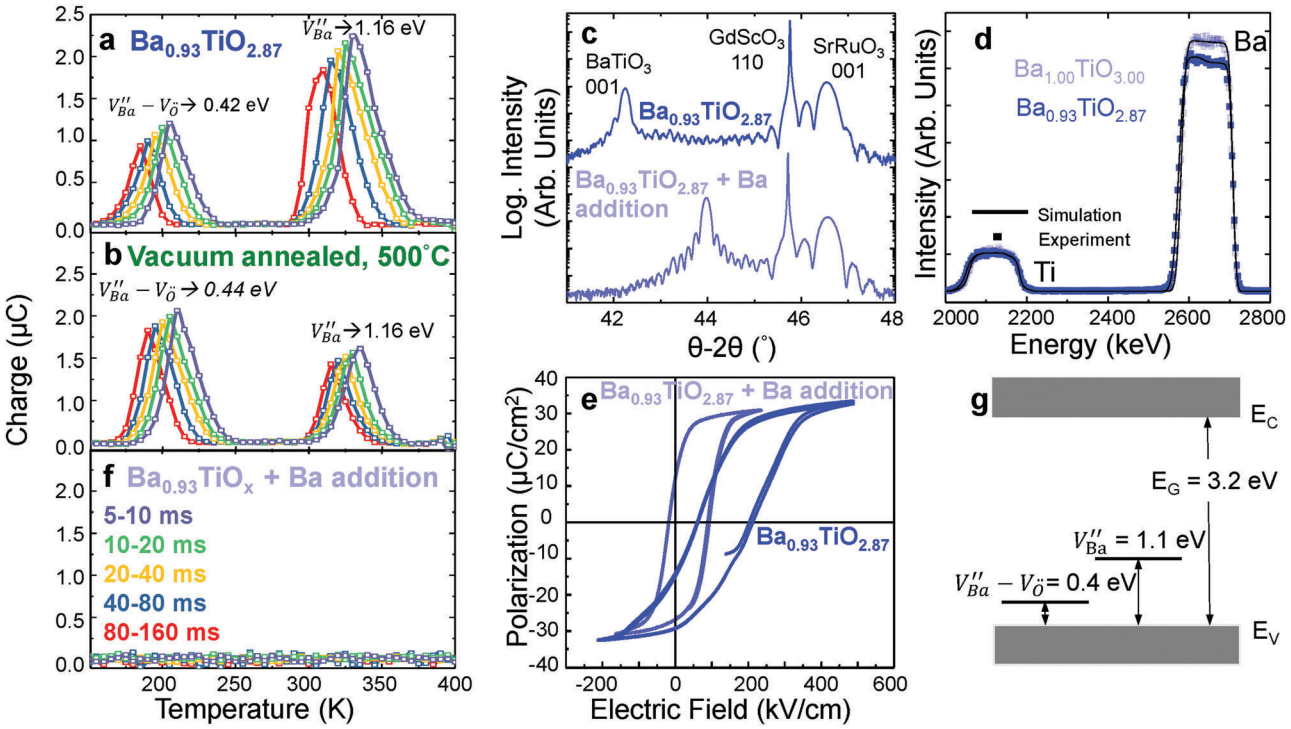

Fig. 5 Deep-level transient spectroscopy data for (a) an as-grown $Ba_{0.93}TiO_{2.87}$ heterostructure, (b) the same film after vacuum annealing at 500 °C, and (f) the same after barium addition *via* the CVD-like process. (c) θ–2θ X-ray diffraction scans of the $Ba_{0.93}TiO_{2.87}$ heterostructure in the (top) as-grown state and (bottom) followed by barium addition *via* the CVD-like process. (d) Rutherford backscattering spectra and (e) polarization–electric field hysteresis loops for the $Ba_{0.93}TiO_{2.87}$ heterostructure in the as-grown state and followed by barium addition *via* the CVD-like process. (g) Schematic of the defect state energies present within the $Ba_{1-x}TiO_y$ films wherein E_G is the band gap of $BaTiO_3$.

formed to compensate for the barium vacancies in the Schottky pairs.[53] From there, we explored the effect of introduction of additional oxygen vacancies by annealing the sample at 500 °C for 60 min at an oxygen pressure of 1 mTorr. After this treatment, a stark change in the DLTS spectra was observed (Fig. 5b) wherein, although the temperatures of occurrence of the two peaks remain the same (implying no change in trap energy), the peak heights changed (implying a change in the concentration of the trap states). The trap ~0.4 eV from the band edge increases in concentration, at the expense of the trap ~1.2 eV from the band edge, which decreases in concentration. This would imply that oxygen vacancies are associated with the shallower trap and not with the deeper trap; this can be explained by the fact that as more oxygen vacancies are introduced, some of the isolated V''_{Ba} values are interconverted into $V''_{Ba} - V^{\bullet\bullet}_{O}$ complexes, thereby changing the relative trap concentrations. Finally, we explored the effect of reintroducing barium into the lattice by annealing the films at 700 °C for 60 min in a barium-rich environment described above. Similar approaches have been used to overcome lead loss in sol–gel $PbZr_{1-x}Ti_xO_3$ films.[56,57] After the experiment, a dramatic change in the structure was observed (Fig. 5c), wherein the hitherto observed ~5.4% expansion of the lattice is reduced to an ~1.1% expansion. Subsequent RBS studies reveal that barium has indeed been reintroduced, and a new film chemistry of $Ba_{1.00}TiO_{3.00}$ is observed (Fig. 5d). As a result, the ferroelectric hysteresis loops of these "healed" films show that the internal bias is greatly reduced and the pinching observed previously is eliminated (Fig. 5e). This suggests that it is possible to almost completely remove the barium vacancies from these films after the fact. Subsequent DLTS studies (Fig. 5f) taken from these healed films show the disappearance of the two peaks observed before. This further supports the attribution of both peaks to the defects noted, in particular that barium vacancies are associated with both the peaks. Finally, taking into account all the measurements performed thus far, we can prepare a proposed band structure for the $Ba_{1-x}TiO_y$ films produced in this study depicting the position of the various intra-gap trap states that are formed by barium and oxygen deficiency (Fig. 5g).

Conclusions

Here, the effects of growth conditions on the film chemistry, structure, electrical leakage, dielectric response, and ferroelectric behavior of $Ba_{1-x}TiO_y$ thin films have been explored. Although single-phase, coherently-strained films are produced in all cases, small variations in the laser fluence during pulsed-laser deposition result in films with chemistries ranging from $BaTiO_3$ to $Ba_{0.93}TiO_{2.87}$. In turn, as the laser fluence increases and the films become more barium and oxygen deficient, the out-of-plane lattice parameter expands (as much as 5.4% beyond the expected value for $BaTiO_3$ films). Stoichiometric

$Ba_{1.00}TiO_{3.00}$ films are found to be three orders of magnitude more conducting than $Ba_{0.93}TiO_{2.87}$ films, and the barium- and oxygen-deficient films exhibit smaller low-field permittivity, lower loss tangents, and higher dielectric maximum temperatures. Although large polarization is observed in all cases, large built-in potentials (shifted loops) and hysteresis-loop pinching are present in the barium- and oxygen-deficient films – suggesting the presence of defect dipoles. The effect of these defects on ferroelectric hysteresis was also studied using FORC studies. Temperature-dependent current–voltage and DLTS studies reveal at least two defect states at $\sim$0.4 eV and $\sim$1.2 eV above the valence band that grows in concentration with increasing deficiency in both barium and oxygen. *Ex situ* introduction of additional oxygen vacancies and barium allows for further understanding of the nature of the defects and their role in driving structural and property evolution. The defect states are attributed to shallow $V''_{Ba} - V^{\bullet\bullet}_{O}$ defect–dipole complexes and deep V''_{Ba} defect states, which can be removed *via ex post facto* processing if desired. Ultimately, such work to understand and control the defects in this important material could provide a pathway to enable better control over its properties and highlight new avenues to manipulate functions in these complex materials.

Conflicts of interest

There are no conflicts to declare.

Acknowledgements

A. D. acknowledges support from the U.S. Department of Energy, Office of Science, Office of Basic Energy Sciences, and the Materials Sciences and Engineering Division under Contract No. DE-AC02-05-CH11231 (Materials Project program KC23MP) for the study of ferroic complex oxides. S. S. acknowledges support from the U.S. Department of Energy, Office of Science, Office of Basic Energy Sciences, under Award Number DE-SC-0012375 for the development of the ferroelectric thin films. R. X. acknowledges support from the National Science Foundation under Grant DMR-1708615. L. R. D. acknowledges support from the National Science Foundation under Grant OISE-1545907. S. P. acknowledges support from the Army Research Office under Grant W911NF-14-1-0104. A. R. D. acknowledges support from the Gordon and Betty Moore Foundation's EPiQS Initiative, under Grant GBMF5307. L. W. M. acknowledges support from the National Science Foundation under Grant DMR-1608938.

References

1 S. Saremi, R. Gao, A. Dasgupta and L. W. Martin, *Am. Ceram. Soc. Bull.*, 2018, **97**, 16–23.
2 T. Kawae, Y. Terauchi, H. Tsuda, M. Kumeda and A. Morimoto, *Appl. Phys. Lett.*, 2009, **94**, 112904.
3 M. Dawber and J. F. Scott, *Appl. Phys. Lett.*, 2000, **76**, 1060–1062.
4 D. M. Smyth, M. P. Harmer and P. Peng, *J. Am. Ceram. Soc.*, 1989, **72**, 2276–2278.
5 H. Kishi, Y. Mizuno and H. Chazono, *Jpn. J. Appl. Phys.*, 2003, **42**, 1.
6 K. Uchino, *Piezoelectric Actuators and Ultrasonic Motors*, Springer Science & Business Media, 1996.
7 S. Wada, S. Suzuki, T. Noma, T. Suzuki, M. Osada, M. Kakihana, S.-E. Park, L. E. Cross and T. R. Shrout, *Jpn. J. Appl. Phys.*, 1999, **38**, 5505.
8 F. D. Morrison, D. C. Sinclair and A. R. West, *J. Appl. Phys.*, 1999, **86**, 6355–6366.
9 V. J. Tennery and R. L. Cook, *J. Am. Ceram. Soc.*, 1961, **44**, 187–193.
10 J. Keeble, S. Wicklein, R. Dittmann, L. Ravelli, R. A. Mackie and W. Egger, *Phys. Rev. Lett.*, 2010, **105**, 226102.
11 T. Ohnishi, M. Lippmaa, T. Yamamoto, S. Meguro and H. Koinuma, *Appl. Phys. Lett.*, 2005, **87**, 241919.
12 A. R. Damodaran, E. Breckenfeld, Z. Chen, S. Lee and L. W. Martin, *Adv. Mater.*, 2014, **26**, 6341–6347.
13 S. Saremi, R. Xu, L. R. Dedon, J. A. Mundy, S.-L. Hsu, Z. Chen, A. R. Damodaran, S. P. Chapman, J. T. Evans and L. W. Martin, *Adv. Mater.*, 2016, **28**, 10750–10756.
14 R. Gao, S. E. Reyes-Lillo, R. Xu, A. Dasgupta, Y. Dong, L. R. Dedon, J. Kim, S. Saremi, Z. Chen, C. R. Serrao, H. Zhou, J. B. Neaton and L. W. Martin, *Chem. Mater.*, 2017, **29**, 6544–6551.
15 L. R. Dedon, S. Saremi, Z. Chen, A. R. Damodaran, B. A. Apgar, R. Gao and L. W. Martin, *Chem. Mater.*, 2016, **28**, 5952–5961.
16 E. Breckenfeld, R. Wilson, J. Karthik, A. R. Damodaran, D. G. Cahill and L. W. Martin, *Chem. Mater.*, 2012, **24**, 331–337.
17 S. Saremi, R. Xu, R. D. Liv, R. Gao, A. Ghosh, A. Dasgupta and L. W. Martin, *Adv. Mater. Interfaces*, 2018, **5**, 1700991.
18 H. Lee, T. H. Kim, J. J. Patzner, H. Lu, J.-W. Lee, H. Zhou, W. Chang, M. K. Mahanthappa, E. Y. Tsymbal, A. Gruverman and C.-B. Eom, *Nano Lett.*, 2016, **16**, 2400–2406.
19 S. Guillemet-Fritsch, Z. Valdez-Nava, C. Tenailleau, T. Lebey, B. Durand and J.-Y. Chane-Ching, *Adv. Mater.*, 2008, **20**, 551–555.
20 H. Han, D. Ghosh, J. L. Jones and J. C. Nino, *J. Am. Ceram. Soc.*, 2013, **96**, 485–490.
21 H. Han, C. Voisin, S. Guillemet-Fritsch, P. Dufour, C. Tenailleau, C. Turner and J. C. Nino, *J. Appl. Phys.*, 2013, **113**, 024102.
22 K. J. Choi, M. Biegalski, Y. L. Li, A. Sharan, J. Schubert, R. Uecker, P. Reiche, Y. B. Chen, X. Q. Pan, V. Gopalan, L.-Q. Chen, D. G. Schlom and C. B. Eom, *Science*, 2004, **306**, 1005–1009.
23 J. Karthik, A. R. Damodaran and L. W. Martin, *Adv. Mater.*, 2012, **24**, 1610–1615.
24 D. V. Lang, *J. Appl. Phys.*, 1974, **45**, 3023–3032.
25 D. Kan and Y. Shimakawa, *Appl. Phys. Lett.*, 2011, **99**, 081907.
26 J. H. Haeni, P. Irvin, W. Chang, R. Uecker, P. Reiche, Y. L. Li, S. Choudhury, W. Tian, M. E. Hawley, B. Craigo, A. K. Tagantsev, X. Q. Pan, S. K. Streiffer, L. Q. Chen,

S. W. Kirchoefer, J. Levy and D. G. Schlom, *Nature*, 2004, **430**, 758.
27 G. Arlt and H. Neumann, *Ferroelectrics*, 1988, **87**, 109–120.
28 K. Carl and K. H. Hardtl, *Ferroelectrics*, 1977, **17**, 473–486.
29 L. Zhang, E. Erdem, X. Ren and R.-A. Eichel, *Appl. Phys. Lett.*, 2008, **93**, 202901.
30 R.-A. Eichel, P. Erhart, P. Träskelin, K. Albe, H. Kungl and M. J. Hoffmann, *Phys. Rev. Lett.*, 2008, **100**, 095504.
31 T. Rojac, S. Drnovsek, A. Bencan, B. Malic and D. Damjanovic, *Phys. Rev. B*, 2016, **93**, 014102.
32 C. R. Pike, *Phys. Rev. B: Condens. Matter Mater. Phys.*, 2003, **68**, 104424.
33 A. P. Roberts, C. R. Pike and K. L. Verosub, *J. Geophys. Res.: Solid Earth*, 2000, **105**, 28461–28475.
34 F. Preisach, *Z. Phys.*, 1935, **94**(5–6), 277–302.
35 A. T. Bartic, D. J. Wouters, H. E. Maes, J. T. Rickes and R. M. Waser, *J. Appl. Phys.*, 2001, **89**, 3420–3425.
36 G. Robert, D. Damjanovic and N. Setter, *Appl. Phys. Lett.*, 2000, **77**, 4413–4415.
37 I. Fujii, M. Ugorek and S. Trolier-McKinstry, *J. Appl. Phys.*, 2010, **107**, 104116.
38 A. Chandrasekaran, D. Damjanovic, N. Setter and N. Marzari, *Phys. Rev. B: Condens. Matter Mater. Phys.*, 2013, **88**, 214116.
39 T. Rojac, M. Kosec, B. Budic, N. Setter and D. Damjanovic, *J. Appl. Phys.*, 2010, **108**, 074107.
40 N.-H. Chan and D. M. Smyth, *J. Am. Ceram. Soc.*, 1984, **67**, 285–288.
41 P. Erhart and K. Albe, *J. Appl. Phys.*, 2008, **104**, 044315.
42 G. V. Lewis and C. R. A. Catlow, *Radiat. Eff.*, 1983, **73**, 307–314.
43 G. V. Lewis and C. R. A. Catlow, *J. Phys. Chem. Solids*, 1986, **47**, 89–97.
44 G. Koschek and E. Kubalek, *Phys. Status Solidi A*, 1983, **79**, 131–139.
45 T.-B. Wu and J.-N. Lin, *J. Am. Ceram. Soc.*, 1994, **77**, 759–764.
46 N.-H. Chan, R. K. Sharma and D. M. Smyth, *J. Am. Ceram. Soc.*, 1981, **64**, 556–562.
47 N. Oshime, J. Kano, N. Ikeda, T. Teranishi, T. Fujii, T. Ueda and T. Ohkubo, *J. Appl. Phys.*, 2016, **120**, 154101.
48 M. V. Raymond and D. M. Smyth, *J. Phys. Chem. Solids*, 1996, **57**, 1507–1511.
49 M. Boswarva and A. B. Lidiard, *Philos. Mag.*, 1967, **16**, 805–826.
50 A. B. Lidiard, *Philos. Mag. A*, 1981, **43**, 291–300.
51 N. G. Eror and U. Balachandran, *Solid State Commun.*, 1982, **44**, 1117–1119.
52 M. Leslie and N. J. Gillan, *J. Phys. C: Solid State Phys.*, 1985, **18**, 973.
53 P. Erhart and K. Albe, *J. Appl. Phys.*, 2007, **102**, 084111.
54 R. H. Bube, *J. Appl. Phys.*, 1962, **33**, 1733–1737.
55 R. L. Angle and H. E. Talley, *IEEE Trans. Electron Devices*, 1978, **25**, 1277–1283.
56 Y. L. Tu and S. J. Milne, *J. Mater. Sci.*, 1995, **30**, 2507–2516.
57 A. I. Kingon and J. B. Clark, *J. Am. Ceram. Soc.*, 1983, **66**, 253–256.